

## HATS-71B: A GIANT PLANET TRANSITING AN M3 DWARF STAR IN TESS SECTOR 1 \*

G. Á. BAKOS,<sup>1,2,†</sup> D. BAYLISS,<sup>3</sup> J. BENTO,<sup>4</sup> W. BHATTI,<sup>1</sup> R. BRAHM,<sup>5,6,7</sup> Z. CSUBRY,<sup>1</sup> N. ESPINOZA,<sup>8,9,10</sup>  
J. D. HARTMAN,<sup>1</sup> TH. HENNING,<sup>8</sup> A. JORDÁN,<sup>7,6</sup> L. MANCINI,<sup>11,8,12</sup> K. PENEV,<sup>13</sup> M. RABUS,<sup>6,8,14</sup> P. SARKIS,<sup>8</sup> V. SUC,<sup>6</sup>  
M. DE VAL-BORRO,<sup>15</sup> G. ZHOU,<sup>16</sup> R. P. BUTLER,<sup>17</sup> J. CRANE,<sup>18</sup> S. DURKAN,<sup>19</sup> S. SHECTMAN,<sup>18</sup> J. KIM,<sup>1</sup> J. LÁZÁR,<sup>20</sup>  
I. PAPP,<sup>20</sup> P. SÁRI,<sup>20</sup> G. RICKER,<sup>21</sup> R. VANDERSPEK,<sup>21</sup> D. W. LATHAM,<sup>16</sup> S. SEAGER,<sup>21</sup> J. N. WINN,<sup>1</sup> J. JENKINS,<sup>22</sup>  
A. D. CHACON,<sup>23</sup> G. FÜRÉSZ,<sup>21</sup> B. GOEKE,<sup>21</sup> J. LI,<sup>22</sup> S. QUINN,<sup>16</sup> E. V. QUINTANA,<sup>24</sup> P. TENENBAUM,<sup>22</sup> J. TESKE,<sup>18</sup>  
M. VEZIE,<sup>21</sup> L. YU,<sup>21</sup> C. STOCKDALE,<sup>25</sup> P. EVANS,<sup>26</sup> AND H. M. RELLES<sup>16</sup>

<sup>1</sup>Department of Astrophysical Sciences, Princeton University, NJ 08544, USA

<sup>2</sup>MTA Distinguished Guest Fellow, Konkoly Observatory, Hungary

<sup>3</sup>Department of Physics, University of Warwick, Coventry CV4 7AL, UK

<sup>4</sup>Research School of Astronomy and Astrophysics, Australian National University, Canberra, ACT 2611, Australia

<sup>5</sup>Center of Astro-Engineering UC, Pontificia Universidad Católica de Chile, Av. Vicuña Mackenna 4860, 7820436 Macul, Santiago, Chile

<sup>6</sup>Instituto de Astrofísica, Pontificia Universidad Católica de Chile, Av. Vicuña Mackenna 4860, 7820436 Macul, Santiago, Chile

<sup>7</sup>Millennium Institute of Astrophysics, Av. Vicuña Mackenna 4860, 7820436 Macul, Santiago, Chile

<sup>8</sup>Max Planck Institute for Astronomy, Königstuhl 17, 69117 - Heidelberg, Germany

<sup>9</sup>Bernoulli Fellow

<sup>10</sup>IAU-Gruber Fellow

<sup>11</sup>Department of Physics, University of Rome Tor Vergata, Via della Ricerca Scientifica 1, I-00133 - Roma, Italy

<sup>12</sup>INAF - Astrophysical Observatory of Turin, Via Osservatorio 20, I-10025 - Pino Torinese, Italy

<sup>13</sup>Department of Physics, University of Texas at Dallas, Richardson, TX 75080, USA

<sup>14</sup>Visiting astronomer, Cerro Tololo Inter-American Observatory, National Optical Astronomy Observatory.

<sup>15</sup>Astrochemistry Laboratory, Goddard Space Flight Center, NASA, 8800 Greenbelt Rd, Greenbelt, MD 20771, USA

<sup>16</sup>Harvard-Smithsonian Center for Astrophysics, 60 Garden St., Cambridge, MA 02138, USA

<sup>17</sup>Department of Terrestrial Magnetism, Carnegie Institution for Science, Washington, DC 20015, USA

<sup>18</sup>The Observatories of the Carnegie Institution for Science, 813 Santa Barbara St, Pasadena, CA 91101, USA

<sup>19</sup>Astrophysics Research Centre, Queens University, Belfast, Northern Ireland, UK

<sup>20</sup>Hungarian Astronomical Association, 1451 Budapest, Hungary

<sup>21</sup>Massachusetts Institute of Technology

<sup>22</sup>SETI Institute/NASA Ames Research Center

<sup>23</sup>Millennium Engineering and Integration Co./NASA Ames Research Center

<sup>24</sup>NASA Goddard Space Flight Center

<sup>25</sup>Hazelwood Observatory, Victoria, Australia

<sup>26</sup>El Sauce Observatory, Chile

### ABSTRACT

We report the discovery of HATS-71b, a transiting gas giant planet on a  $P = 3.7955$  day orbit around a  $G = 15.35$  mag M3 dwarf star. HATS-71 is the coolest M dwarf star known to host a hot Jupiter. The loss of light during transits is 4.7%, more than any other confirmed transiting planet system. The planet was identified as a candidate by the ground-based HATSouth transit survey. It was confirmed using ground-based photometry, spectroscopy, and imaging, as well as space-based photometry from the NASA *TESS* mission (TIC 234523599). Combining all of these data, and utilizing Gaia DR2, we find that the planet has a radius of  $1.080 \pm 0.016 R_J$  and mass of  $0.45 \pm 0.24 M_J$  (95% confidence

Corresponding author: Gáspár Bakos  
gbakos@astro.princeton.edu

\* The HATSouth network is operated by a collaboration consisting of Princeton University (PU), the Max Planck Institute für Astronomie (MPIA), the Australian National University (ANU), and the Pontificia Universidad Católica de Chile (PUC). The station at Las Campanas Observatory (LCO) of the Carnegie Institute is operated by PU in conjunction with PUC, the station at the High Energy Spectroscopic Survey (H.E.S.S.) site is operated in conjunction with MPIA, and the station at Siding Spring Observatory (SSO) is operated jointly with ANU. This paper includes data gathered with the 6.5 meter Magellan Telescopes at Las Campanas Observatory, Chile.

upper limit of  $0.81 M_J$ ), while the star has a mass of  $0.569_{-0.069}^{+0.042} M_\odot$  and a radius of  $0.5161_{-0.0099}^{+0.0053} R_\odot$ . The Gaia DR2 data show that HATS-71 lies near the binary main sequence in the Hertzsprung-Russell diagram, suggesting that there may be an unresolved stellar binary companion. All of the available data is well fitted by a model in which there is a secondary star of mass  $0.24 M_\odot$ , although we caution that at present there is no direct spectroscopic or imaging evidence for such a companion. Even if there does exist such a stellar companion, the radius and mass of the planet would be only marginally different from the values we have calculated under the assumption that the star is single.

*Keywords:* planetary systems — stars: individual ( HATS-71, GSC ) techniques: spectroscopic, photometric

## 1. INTRODUCTION

Much has been learned about the physical properties of exoplanets in the nearly three decades following the discovery of the exoplanet candidate HD 114762 b (Latham et al. 1989). As of 2018 September 27, the NASA Exoplanet Archive lists 3791 confirmed and validated exoplanets, the majority of which were found by the NASA *Kepler* mission via the transit method. Among the confirmed planets are 418 short-period gas giant planets ( $P < 10$  days, and  $M_p > 0.2 M_J$  or  $R_p > 0.7 R_J$ ). These are the so-called hot-Jupiters. Especially important are the 375 hot Jupiters which are known to transit their host stars. These objects are among the best-studied planets, providing a wealth of information about their physical properties. Among the 270 planets for which the mass and radius have both been determined with a precision of 20% or better, 235 are hot Jupiters. Of the 133 planets for which the (sky projected) stellar obliquity has been measured, 117 are hot Jupiters (TEPCat; Southworth 2011). Similarly, the majority of exoplanets with observational constraints on the properties of their atmospheres are hot Jupiters (e.g., Madhusudhan 2018). All of these observations have been greatly facilitated by the frequently occurring and deep ( $\sim 1\%$ ) transits presented by these systems.

All but twelve of the 418 hot Jupiters in the NASA Exoplanet Archive have been found around F, G or K-type host stars ( $4000 \text{ K} < T_{\text{eff}} < 7300 \text{ K}$ , or  $0.6 M_{\odot} < M < 1.6 M_{\odot}$  if  $T_{\text{eff}}$  is not given in the database). One of the hot Jupiters in this sample is around a B-star, seven are around A stars, and only four have been found around M dwarf stars. The hot Jupiters that have previously been discovered around M dwarf stars include Kepler-45 b ( $M_p = 0.505 \pm 0.090 M_J$ ,  $M_S = 0.59 \pm 0.06 M_{\odot}$ ,  $T_{\text{eff}} = 3820 \pm 90 \text{ K}$  Johnson et al. 2012), HATS-6 b ( $M_p = 0.319 \pm 0.070 M_J$ ,  $M_S = 0.574_{-0.027}^{+0.020} M_{\odot}$ ,  $T_{\text{eff}} = 3724 \pm 18 \text{ K}$  Hartman et al. 2015), NGTS-1 b ( $M_p = 0.812_{-0.075}^{+0.066} M_J$ ,  $M_S = 0.617_{-0.062}^{+0.023} M_{\odot}$ ,  $T_{\text{eff}} = 3916_{-63}^{+71} \text{ K}$  Bayliss et al. 2018), and HD 41004 B b ( $M_p \sin i = 18.37 \pm 0.22 M_J$ ,  $M_S \sim 0.4 M_{\odot}$  Zucker et al. 2003). The latter object was detected in the radial velocity (RV) observations of the M2V component of a K1V+M2V visual binary, and the inferred  $19 M_J$  brown-dwarf companion mass is a lower limit. The other three objects are transiting systems.

Theoretical models of planet formation and evolution have predicted that hot Jupiters should be less common around M dwarf stars than around solar-type stars (Mordasini et al. 2012). While there is some observational support for this prediction from RV surveys (Johnson et al. 2010), the number of M dwarfs that have

been systematically surveyed for hot Jupiters is still too low to be certain of this conclusion (Obermeier et al. 2016).

One of the main goals in current exoplanet research is to expand the sample of well-characterized hot Jupiters known around M dwarfs and A or earlier-type stars. This will allow the occurrence rate of hot Jupiters to be measured as a function of stellar mass, and will also enable the dependence of other planetary system properties on stellar mass to be studied. Some of these properties that might be investigated include the orbital obliquities of the planets, the degree of inflation in the planetary radii, and the atmospheric properties of the planets.

Giant planets transiting M dwarf stars also provide at least two observational advantages over similar-size planets transiting larger stars. They produce very deep transits. In principle, a giant planet could completely obscure a very low-mass star, although no such system has been discovered to date. The deep transits allow for observations with a higher signal-to-noise ratio (S/N), especially if conducted in the IR where the stars have a higher photon flux density. The stars themselves undergo very little evolution over the lifetime of the Galaxy, enabling a more precise constraint on the mass and radius of the star (and hence of the planet) from the available observations compared to what can be done for more massive stars (e.g., Hartman et al. 2015).

The primary challenge in discovering transiting hot Jupiters around M dwarfs is the faintness of these stars. In order to survey a sufficient number of M dwarfs to detect the rare cases of transiting hot Jupiters, it is necessary to observe stars down to  $V \sim 15$  mag, which is fainter than the limits of many of the ground-based transit surveys that have been productive at discovering transiting hot Jupiters. The two ground-based surveys which have discovered transiting hot Jupiters around M dwarfs are the HATSouth survey (Bakos et al. 2013) and the NGTS survey (Wheatley et al. 2018). Both of these projects use larger aperture telescopes compared to the other wide-field transit surveys (0.18 m in the case of HATSouth and 0.20 m in the case of NGTS) allowing for greater sensitivity to M dwarf stars.

In this paper we present the discovery of HATS-71b by the HATSouth survey, the fifth hot Jupiter found around an M dwarf star, and the fourth transiting system of this type. With a spectroscopic effective temperature of  $3500 \pm 120 \text{ K}$ , and a spectral type of M3V, HATS-71 is the coolest M dwarf known to host a transiting hot Jupiter. The 4.7% deep transits are also the deepest of any transiting system discovered to date. The

planet was first detected by HATSouth, and then confirmed using ground-based spectroscopic and photometric follow-up. It was also recently observed in Sector 1 of the NASA *Transiting Exoplanet Survey Satellite* mission (*TESS*, Ricker et al. 2015), and included in the first set of alerts released to the public. In this paper we present all of these data and analyze them to determine the physical properties of the planet HATS-71b and its host star HATS-71. We also present evidence, driven largely by observations from the Gaia DR2 mission (Gaia Collaboration et al. 2016, 2018), that the planet host may have an unresolved binary star companion with a current projected physical separation of less than 14 AU. If confirmed, the presence of this companion might be responsible for shrinking the orbit of the gas giant planet to its current short period orbit.

In Section 2 we present the observations. We describe the analyses that we have performed to confirm the planetary system and determine its properties in Section 3. We conclude with a discussion of the results in Section 4.

## 2. OBSERVATIONS

### 2.1. Photometric detection

HATS-71 was initially detected as a transiting planet candidate based on observations by the HATSouth network. A total of 26,668 observations were gathered at 4 min cadence between UT 2011 July 17 and UT 2012 October 25. The source was observed by the HS-1, HS-3 and HS-5 instruments (located in Chile, Namibia, and Australia, respectively) in HATSouth field G755, and by the HS-2, HS-4 and HS-6 instruments (located in Chile, Namibia, and Australia, respectively) in HATSouth field G756. Observations were carried out as described by Bakos et al. (2013), and reduced to trend-filtered light curves (filtered using the method of Kovács et al. 2005) and searched for transiting planet signals (using the Box-fitting Least Squares or BLS method; Kovács et al. 2002) as described by Penev et al. (2013). We identified a periodic box-shaped transit signal in the trend-filtered light curve of HATS-71 with a period of 3.7955 days and a depth of 61.8 mmag. Based on this we selected the object as a candidate, assigning it the HATSouth candidate identifier HATS755-002. The trend-filtered HATSouth light curve has a residual RMS of 50 mmag. The light curve is shown phase-folded in Figure 1, while the data are made available in Table 1.

We searched for additional periodic signals in the combined HATSouth light curve using both the Generalized Lomb-Scargle periodogram (Zechmeister & Kürster 2009) and the BLS algorithm, in both cases applied to the light curve after subtracting the best-fit transit model for HATS-71b. We find a peak in the GLS

periodogram at a period of  $41.72 \pm 0.14$  days with a false alarm probability of  $10^{-31}$  (Figure 2). This false alarm probability is estimated using the relations from (Zechmeister & Kürster 2009) appropriate for Gaussian white-noise, but calibrated to the observed sampling and magnitude distribution via bootstrap simulations. The signal is independently detected in the G755 and G756 HATSouth light curves (with peak periods of 37.02 days and 41.86 days, and false alarm probabilities of  $10^{-10}$  and  $10^{-15}$ , respectively), which have similar time-coverage but were obtained with different instruments using different pointings on the sky. Fitting a sinusoid to the phase-folded data yields a semi-amplitude of  $0.0134 \pm 0.0039$  mag. We interpret this period as the photometric rotation period of the star. Given the measured rotation period and stellar radius, the spectroscopic  $v \sin i$  should be  $< 0.625 \text{ m s}^{-1}$ , i.e., undetectable even with the current high-resolution spectroscopy. Both the period and amplitude are typical values for a field M3 dwarf star. No additional significant transit signals are detected by BLS in the combined HATSouth light curve. The highest peak in the spectrum has a period of 82.7 days, a transit depth of 8.5 mmag and a signal-to-noise of only 4.5.

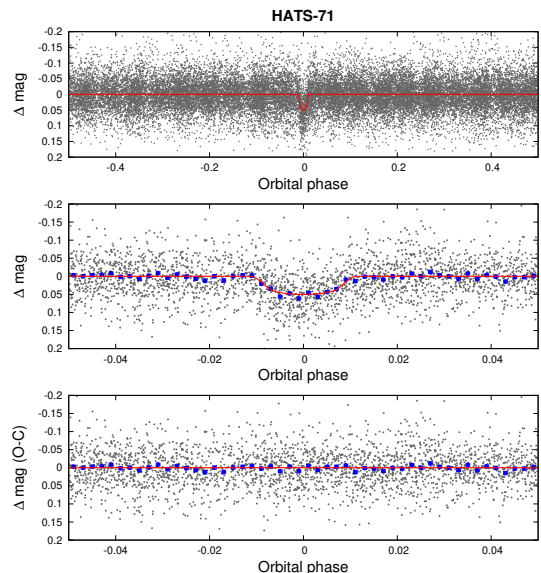


**Figure 1.** Phase-folded unbinned HATSouth light curve for HATS-71. *Top:* the full light curve. *Middle:* the light curve zoomed-in on the transit. *Bottom:* the residuals from the best-fit model zoomed-in on the transit. The solid line shows the model fit to the light curve. The dark filled circles show the light curve binned in phase with a bin size of 0.002.

### 2.2. Spectroscopic Observations

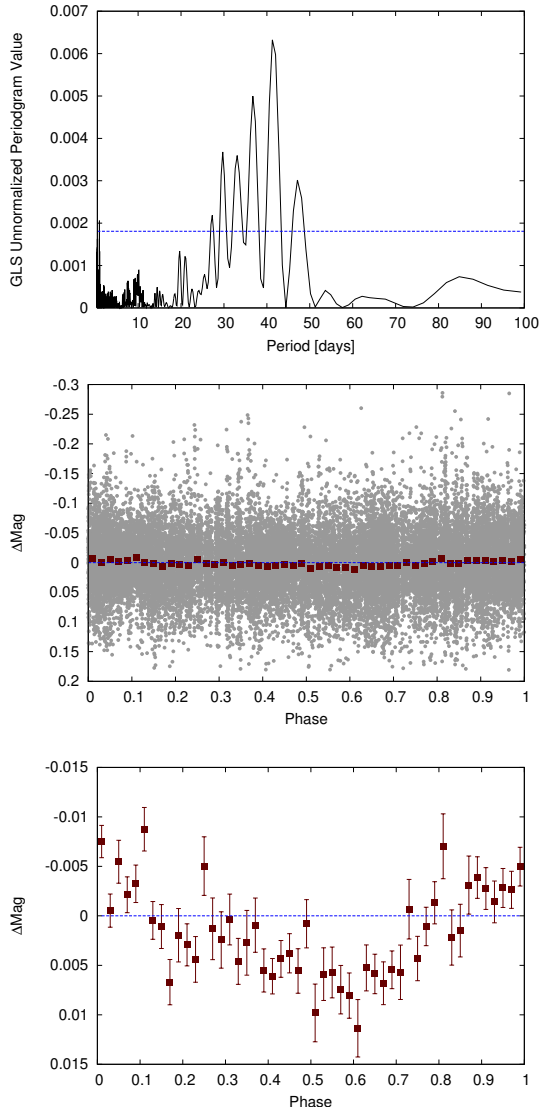


**Figure 2.** *Top:* Generalized Lomb-Scargle (GLS) periodogram of the combined HATSouth light curve after subtracting the best-fit transit model for HATS-71b. The horizontal dashed blue line shows the  $10^{-5}$  false alarm probability level. *Middle:* The HATSouth light curve phase-folded at the peak GLS period of 41.72 days. The gray points show the individual photometric measurements, while the dark red filled squares show the observations binned in phase with a bin size of 0.02. *Bottom:* Same as the middle, here we restrict the vertical range of the plot to better show the variation seen in the phase-binned measurements.

Spectroscopic follow-up observations of HATS-71 were obtained with WiFeS on the ANU 2.3 m (Dopita et al. 2007), PFS on the Magellan 6.5 m (Crane et al. 2006, 2008, 2010), and ARCoIRIS on the Blanco 4 m telescope (Abbott et al. 2016a). The target was also observed with FEROS on the MPG 2.2 m (Kaufer & Pasquini 1998)

between 2016 July 1 and 2016 September 16, but the spectra were all too low S/N to be of use.

The WiFeS observations of HATS-71, which were reduced following Bayliss et al. (2013), were used for reconnaissance of this faint M dwarf. We obtained a single spectrum at resolution  $R \equiv \Delta \lambda / \lambda \approx 3000$  and S/N per resolution element of 18.9 on UT 2014 August 6 (Figure 3). We used this observation to estimate the atmospheric parameters of the star. The classification pipeline described by Bayliss et al. (2013) yielded parameters of  $T_{\text{eff},*} = 3500 \pm 300$  K,  $\log g = 4.7 \pm 0.3$  (cgs), and  $[\text{Fe}/\text{H}] = 0.0 \pm 0.5$  dex, however a comparison to M dwarf standards indicates a somewhat lower temperature (Figure 3). Based on spectral matching to BT-Settl models (Allard et al. 2011) we estimate a temperature of 3350 K. The spectrum reveals this object to be a single-lined mid-M dwarf star with  $v \sin i < 50$  km s $^{-1}$ . We also obtained four spectra at a resolution of  $R \approx 7000$  between 2014 August 6–9 which we used to check for any large amplitude RV variations. The spectra have a S/N between 5.9 and 21.2. The resulting radial velocities have good phase coverage and an RMS scatter of 2.3 km s $^{-1}$ , comparable to the median per-point uncertainty of 2.9 km s $^{-1}$ . The resulting upper limit on the mass of the transiting companion is  $M_p < 31 M_J$  at  $3\sigma$  confidence.

A total of eight PFS observations were obtained for HATS-71 between 2014 December 31 and 2017 January 13. These include seven observations through an I<sub>2</sub> absorption cell, and one observation without the cell used to construct a template spectrum for use in the RV measurements. The observations were reduced to high-precision relative RV measurements following Butler et al. (1996), while spectral line bisector spans (BSs) and their uncertainties were measured as described by Jordán et al. (2014) and Brahm et al. (2017a). To avoid excessive cosmic ray contamination and smearing due to changes in time in the barycentric velocity correction, each observation was composed of two to four exposures which were independently reduced and then co-added. The high-precision RV and BS measurements are given in Table 5, and are shown phase-folded, together with the best-fit model, in Figure 4. Due to the faintness of the source, the RVs have a median per-point uncertainty of 17 ms $^{-1}$ , which may be underestimated. The residuals from the best-fit model have an RMS of 89 ms $^{-1}$  (the observations themselves have an RMS of 106 ms $^{-1}$ ). The BS measurements have an even larger scatter of 1.6 km s $^{-1}$ , limiting their use in excluding blended eclipsing binary scenarios (such scenarios are considered and rejected in Section 3.2).

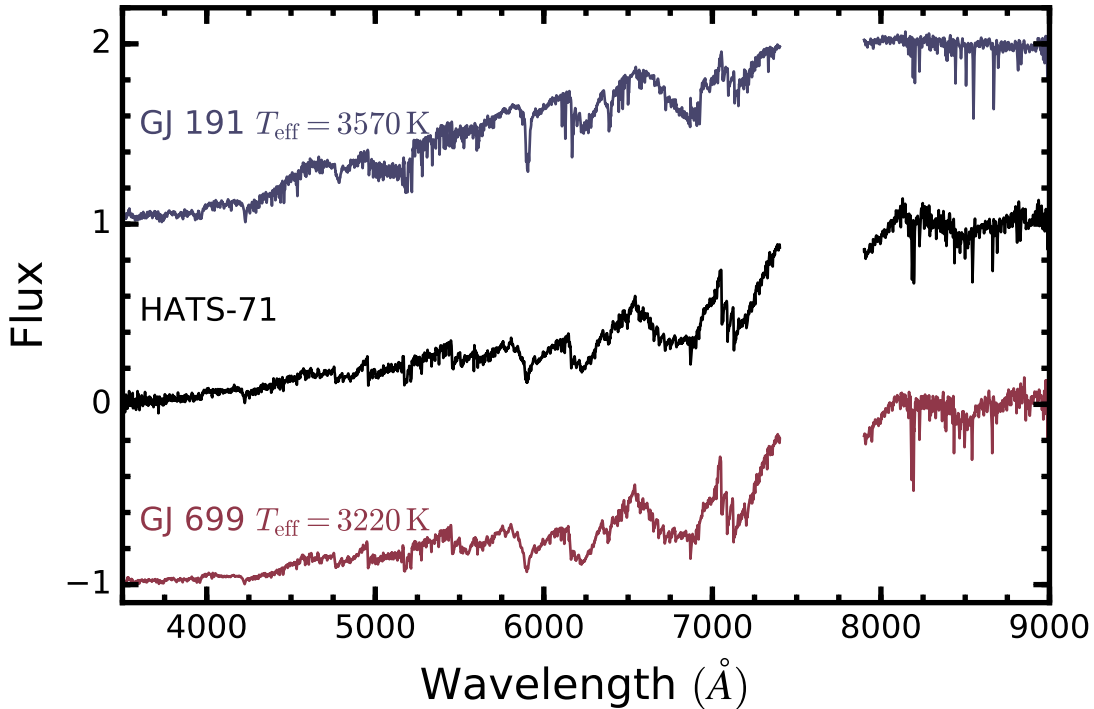


**Figure 3.** WiFeS/ANU 2.3 m  $R = 3000$  optical spectra of HATS-71 (middle spectrum) and two other M dwarf standard stars for comparison. HATS-71 has the optical spectrum of an M3 dwarf star. The relative fluxes are on an arbitrary scale, and the two standard stars have been shifted vertically for clarity.

We checked the PFS observations for  $H\alpha$  emission, indicative of chromospheric activity, and found no evidence for this. If anything,  $H\alpha$  is seen in absorption in these spectra.

The surface temperature of HATS-71 is too low to apply ZASPE (Brahm et al. 2017b), a synthetic-template-cross-correlation-based method to determine precise stellar atmospheric parameters, which we have used in analyzing most of the other planetary hosts discovered by HATSouth. For this reason we obtained a near-infrared spectrum of HATS-71 using the “Astronomy Research using the Cornell Infra Red Imaging Spectrograph” (ARCoIRIS) instrument on the Blanco 4 m at CTIO (Abbott et al. 2016b). This spectrum was used to determine  $T_{\text{eff}\star}$  and  $[\text{Fe}/\text{H}]$ .

ARCoIRIS is a cross-dispersed, single-object, long-slit, near-infrared spectrograph covering most of the wavelength range from 0.8 to 2.47  $\mu\text{m}$ , at a resolution of roughly 3500. ARCoIRIS spectra can only be taken in a single setup with a fixed slit assembly of  $1''.1 \times 28''$ . We observed HATS-71 using a pair of ABBA patterns (eight 100 s exposures in total) interleaved with hollow cathode lamp spectra, and using HD 1860 as a telluric standard. The observations were carried out on UT 2016 July 15, and were reduced to wavelength- and telluric-corrected

spectra using the standard SPEX-tool package (Cushing et al. 2004; Vacca et al. 2004). We note, that we did not attempt to flux calibrate our spectrum as the observing conditions were not photometric. The data reduction resulted in six extracted orders, though we did not consider the sixth order in our analysis. Finally, we cut out regions strongly affected by telluric lines, normalized the spectra and removed a 2nd order polynomial fit.

In order to estimate  $T_{\text{eff}\star}$  and  $[\text{Fe}/\text{H}]$  from our NIR spectrum, we used the procedure described by Newton et al. (2015). These relations were calibrated using IRTF/Spex spectra with a resolution of  $R \sim 2,000$ , but ARCoIRIS has a resolution of  $R \sim 3,500$ , therefore we downgraded our ARCoIRIS spectra to the IRTF/Spex resolution. In these downgraded spectra we measured the equivalent width (EW) of some selected lines and applied the relation from Newton et al. (2015). Based on this we measure  $T_{\text{eff}\star} = 3500 \pm 120$  K, and  $[\text{Fe}/\text{H}] = 0.26 \pm 0.13$ .

### 2.3. Ground-Based photometric follow-up observations

Follow-up higher-precision ground-based photometric transit observations were obtained for HATS-71 using the Danish 1.54 m telescope at La Silla Observatory in Chile (Andersen et al. 1995), 1 m telescopes from the Las Cumbres Observatory (LCOGT) network (Brown et al.

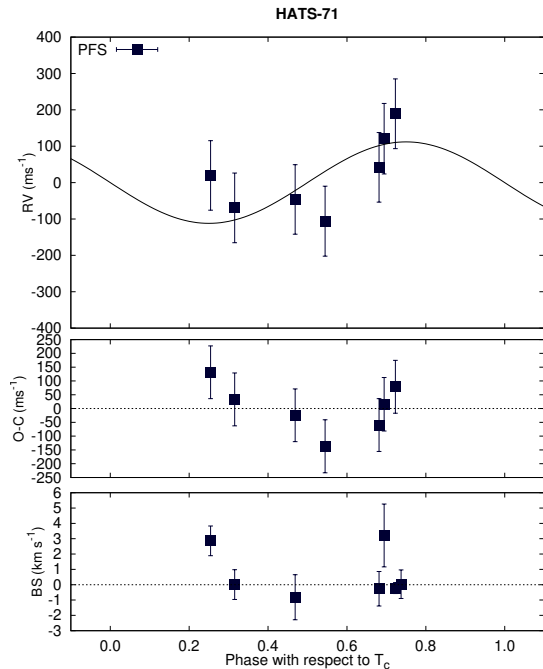


**Figure 4.** Phased high-precision RV measurements from PFS for HATS-71. *Top:* the phased measurements together with our best-fit model (see Table 4). Zero-phase corresponds to the time of mid-transit. The center-of-mass velocity has been subtracted. *Middle:* the velocity  $O-C$  residuals from the best fit. The error bars include the jitter term listed in Table 4 added in quadrature to the formal errors. *Bottom:* the phased bisector spans (BS). Note the different vertical scales of the panels.

2013), a 0.32 m telescope at Hazelwood Observatory in Victoria, Australia, and a 0.36 m telescope at El Sauce Observatory in Chile. Three of the light curves were obtained through the *TESS* Follow-up Program (TFOP) following the independent detection of HATS-71 as a candidate transiting planet system by the *TESS* team (see Section 2.4). All of the ground-based follow-up light curves are shown in Figure 5, while the data are available in Table 1.

An egress event was observed with the DFOSC camera on the DK 1.54 m telescope on the night of UT 2014 Oct 5. A total of 51 images were collected at a median cadence of 225 s. The observations were carried out and reduced to a relative light curve following Rabus et al. (2016). The residuals from the best-fit transit model have a point-to-point RMS of 2.4 mmag.

An ingress event was observed with the SBIG camera on one of the LCOGT 1 m telescopes at the South African Astronomical Observatory (SAAO) on UT 2014 Oct 24. A total of 39 images were collected at a median cadence of 76 s. We also observed a full transit with the sinistro camera on one of the LCOGT 1 m telescopes

at Cerro Tololo Inter-American Observatory (CTIO) in Chile on UT 2014 Nov 9. A total of 56 images were collected at a median cadence of 227 s. These observations were reduced to relative light curves as described in Hartman et al. (2015). A full transit was also observed through the TFOP program using the sinistro camera on one of the LCOGT 1 m telescopes at CTIO on UT 2018 Sep 17. A total of 44 images were collected at a median cadence of 163 s. These data were reduced to aperture photometry using the AstroImageJ software package (AIJ Collins & Kielkopf 2013; Collins et al. 2017). The residuals from the best-fit transit model have a point-to-point RMS of 15 mmag, 3.4 mmag, and 4.6 mmag, on each of the respective nights.

An egress event was observed on UT 2018 Sep 13 at Hazelwood Observatory, a backyard observatory operated by Chris Stockdale in Victoria, Australia. The observations were carried out using a 0.32 m Planewave CDK12 telescope and an SBIG STT-3200 CCD imager. The images had a pixel scale of  $1''.1$ , while the average estimated PSF FWHM on the night of the observations was  $9''$ . We include in the analysis the photometry measured from 28 images collected at a median cadence of 314 s. Aperture photometry was performed using AIJ. The residuals from the best-fit transit model have a point-to-point RMS of 15 mmag.

A full transit was observed on UT 2018 Sep 17 at El Sauce Observatory in Chile by Phil Evans using a 0.36 m Planewave CDK14 telescope and a SBIG STT1603-3 CCD imager. These images had a pixel scale of  $1''.47$ , while the average estimate PSF FWHM on the night of the observations was  $8.2''$ . A total of 90 images are included in the analysis. The median cadence was 185 s. Aperture photometry was performed using AIJ. The residuals from the best-fit transit model have a point-to-point RMS of 11 mmag.

#### 2.4. Space-Based photometric follow-up observations

Photometric time-series observations of HATS-71 were carried out by the NASA *TESS* mission between 2018 July 25 and 2018 August 22 (Sector 1 of the mission). The target (TIC 234523599) was selected for observations at 2-minute cadence through the *TESS* Guest Observer program<sup>1</sup>. The data were processed, and the source was identified as a candidate transiting planet system (denoted TOI 127.01) by the *TESS* team following the methods described by Huang et al. (2018). We note that the identification of this object as a candidate by the *TESS* team was made independently

<sup>1</sup> Program G011214, PI Bakos, "TESS Observations Of Transiting Planet Candidates From HAT"

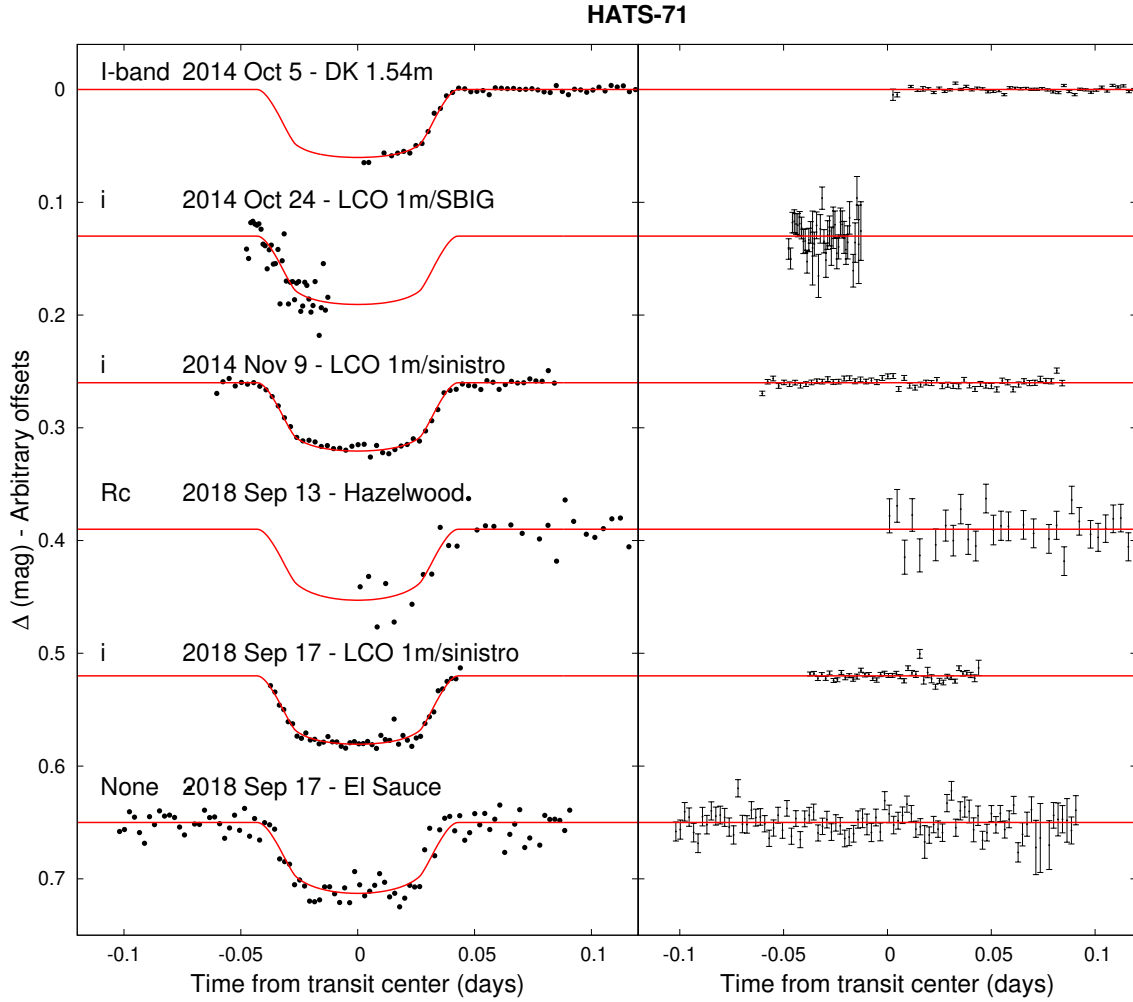


**Figure 5.** Unbinned, de-trended, ground-based, follow-up transit light curves for HATS-71. The dates of the events, filters and instruments used are indicated. Light curves following the first are displaced vertically for clarity. Our best fit from the global modeling described in Section 3.1 is shown by the solid lines. The residuals from the best-fit model are shown on the right-hand-side in the same order as the original light curves. The error bars represent the photon and background shot noise, plus the readout noise.

of the observations described in the previous sections. Here we make use of the preliminary de-trended light curve for HATS-71 produced by the *TESS* Science Processing Operations Center pipeline (based on Jenkins et al. 2016) which was included in the set of *TESS* alerts released to the public on 2018 September 5. Note that these Presearch Data Conditioning (PDC) light curves have not been arbitrarily detrended, but rather have had instrumental systematic signatures identified and removed using a multi-scale, Maximum A Posteriori (msMAP) approach (Stumpe et al. 2014; Smith et al. 2012). A total of 8 consecutive primary transits, and 6 epochs of secondary eclipse are included in the light curve. The residuals from the best-fit model have a point-to-point RMS of 16.5 mmag. The light curve is

shown, together with the best-fit model, in Figure 6, while the time-series data are included in Table 1.

We searched for additional periodic signals in the *TESS* light curve in the same manner as we did for the HATSouth data (Section 2.1). No significant signals were found with either GLS or BLS in the *TESS* light curve after subtracting the best-fit transit model for HATS-71b. No evidence for the  $41.72 \pm 0.14$  day photometric rotation period seen with HATSouth is observed in the *TESS* data, though this is hardly surprising as this period exceeds the duration of the *TESS* observations, and a long-term linear or quadratic trend could have been filtered out by the PDC pipeline. The highest peak in the BLS spectrum of the *TESS* residuals has a period of 9.06 days, a depth of 3.4 mmag and a signal-to-pink-noise ratio of only 5.4.



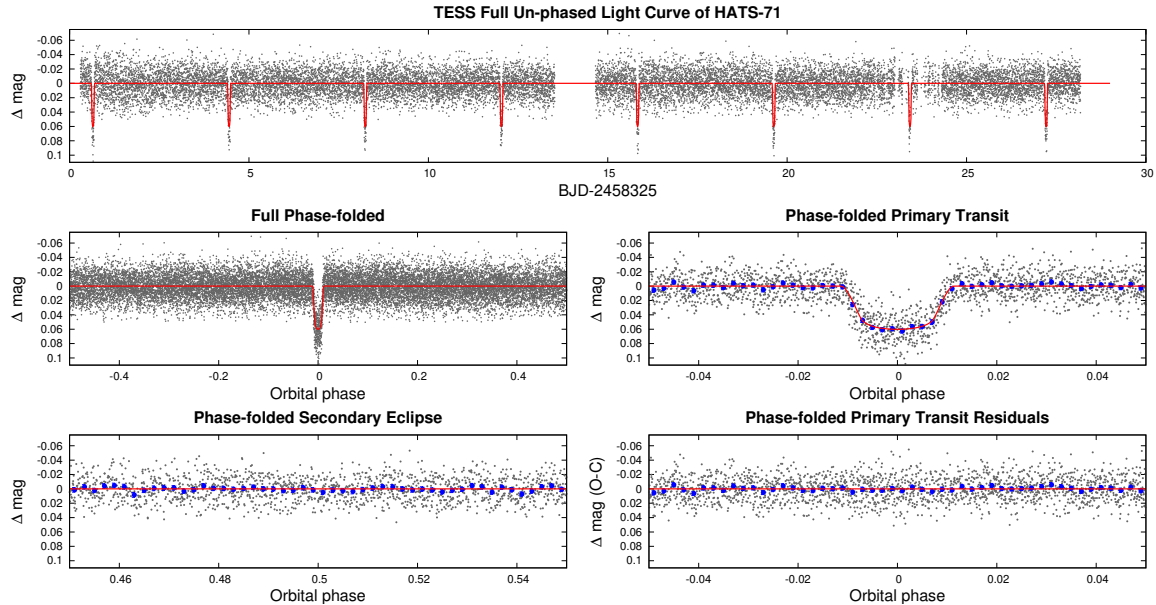


**Figure 6.** *TESS* unbinned light curve for HATS-71. We show the full un-phased light curve as a function of time (*top*), the full phase-folded light curve (*middle left*), the phase-folded light curve zoomed-in on the primary transit (*middle right*), the phase-folded light curve zoomed-in on the secondary eclipse (*bottom left*), and the residuals from the best-fit model, phase-folded and zoomed-in on the primary transit (*bottom right*). The solid line in each panel shows the model fit to the light curve. The dark filled circles show the light curve binned in phase with a bin size of 0.002.

### 2.5. Search for Resolved Stellar Companions

In order to detect neighboring stellar companions we obtained  $z'$ -band high-spatial-resolution lucky imaging observations with the Astralux Sur imager (Hippler et al. 2009) on the New Technology Telescope (NTT) on the night of 2015 December 23. The observations were reduced as in Espinoza et al. (2016), and no neighbors were detected. The effective FWHM of the reduced image is  $46.3 \pm 5.5$  mas. Figure 7 shows the resulting  $5\sigma$  contrast curve. We may exclude neighbors with  $\Delta z' < 2.5$  mag at  $0''.2$ , and  $\Delta z' < 3.2$  mag at  $1''$ . We also note that there are no neighbors within  $10''$  of HATS-71 in the Gaia DR2 catalog, based on which we rule out neighbors with  $G \lesssim 20$  mag down to a limiting resolution of  $\sim 1''$  (e.g., Ziegler et al. 2018).

## 3. ANALYSIS

### 3.1. Joint Modeling of Observations

We analyzed the photometric and spectroscopic observations of HATS-71 following Hartman et al. (2018). In this case we make use of the empirical method for determining the masses and radii of the host stars described in that paper, which is similar to the method proposed by Stassun et al. (2018). The method jointly fits all of the light curves, the RV observations, the Gaia DR2 parallax, the Gaia DR2 and 2MASS broad-band photometry, and the spectroscopically determined  $T_{\text{eff}\star}$  and  $[\text{Fe}/\text{H}]$  (here we use the values determined from the

ARCoIRIS observations, Section 2.2). We adopt a Keplerian orbit to model the RV observations and Mandel & Agol (2002) light curve models in fitting the light curves, and assume fixed quadratic limb darkening coefficients taken from Claret (2004) for  $T_{\text{eff}\star} = 3500$  K and  $\log g = 4.5$  (for the *TESS* light curve we adopt the *I*-band coefficients). We used a Differential Evolution Markov Chain Monte Carlo (DEMCMC) procedure to explore the fitness landscape and to determine the posterior distribution of the parameters.

This modeling allows us to directly determine the radius of the star (making use of bolometric corrections determined from the PARSEC stellar evolution models, Marigo et al. 2017; and using the MWDUST model of Bovy et al. 2016 to place a prior on the extinction). Combining this with the density determined from the transits allows us to then directly measure the mass of the star as well. In Hartman et al. (2018) we found that this empirical method, when applied to the planetary systems HATS-60 through HATS-69, failed to provide reasonably tight constraints on the stellar masses. In the case of HATS-71, however, the observational constraints on the stellar density are more stringent, allowing a significantly tighter constraint on the stellar mass.

In carrying out the analysis we assumed a circular orbit. Note that if the orbit is eccentric, the stellar density inferred from the light curve would be systematically different from what we measured here, which would in turn affect the stellar mass measurement and the in-

**Table 1.** Light curve data for HATS-71.

BJD <sup>a</sup> (2,400,000+)	Mag <sup>b</sup>	$\sigma_{\text{Mag}}$	Mag(orig) <sup>c</sup>	Filter	Instrument
56194.46534	14.46785	0.02515	-0.05133	<i>r</i>	HS/G755.4
56183.07906	14.53916	0.02462	0.01998	<i>r</i>	HS/G755.4
56202.05668	14.48734	0.03641	-0.03184	<i>r</i>	HS/G755.4
56167.89733	14.49451	0.02565	-0.02467	<i>r</i>	HS/G755.4
56141.32989	14.51297	0.03681	-0.00621	<i>r</i>	HS/G755.4
56213.44497	14.51480	0.02061	-0.00438	<i>r</i>	HS/G755.4
56114.76192	14.58036	0.04107	0.06118	<i>r</i>	HS/G755.4
56186.87727	14.53484	0.02796	0.01566	<i>r</i>	HS/G755.4
56145.12690	14.46642	0.02888	-0.05276	<i>r</i>	HS/G755.4
56167.90064	14.51266	0.02463	-0.00652	<i>r</i>	HS/G755.4

<sup>a</sup> Barycentric Julian Date computed on the TDB system with correction for leap seconds.

<sup>b</sup> The out-of-transit level has been subtracted. For observations made with the HATSouth instruments (identified by “HS” in the “Instrument” column) these magnitudes have been corrected for trends using the EPD and TFA procedures applied *prior* to fitting the transit model. This procedure may lead to an artificial dilution in the transit depths when used in its plain mode, instead of the signal reconstruction mode (Kovács et al. 2005). The blend factors for the HATSouth light curves are listed in Table 4. For observations made with follow-up instruments (anything other than “HS” in the “Instrument” column), the magnitudes have been corrected for a quadratic trend in time, and for variations correlated with up to three PSF shape parameters, fit simultaneously with the transit.

<sup>c</sup> Raw magnitude values without correction for the quadratic trend in time, or for trends correlated with the seeing. These are only reported for the follow-up observations.

NOTE— This table is available in a machine-readable form in the online journal. A portion is shown here for guidance regarding its form and content.

ferred planetary mass limits. A solution can be found, for example, with  $e = 0.413$  which passes nicely through the RV observations and is consistent with the host star having a mass and radius of  $0.46 M_{\odot}$  and  $0.45 R_{\odot}$ , respectively, and the planet having a mass and radius of  $1.68 M_J$  and  $0.94 R_J$ , respectively. The limited number of RV observations gathered, however, prevents us from putting a believable constraint on the eccentricity from the data. Additional RV measurements are required, but are expensive due to the faintness of the host star.

In fitting the DK 1.54 m follow-up light curve we included the light curves for 10 neighboring stars as TFA templates to account for systematic drifts in the photometry shared by some of the comparisons that were not well modeled by a simple function of time. For the

other ground-based follow-up light curves, where systematic variations were less pronounced, we included only a quadratic function in time to account for trends.

We also attempted to model the observations using the stellar isochrone-based analysis method described by Hartman et al. (2018). We found, however, that the PARSEC theoretical model does not reproduce the high-precision measurements of color, density and absolute magnitude that are available for HATS-71.

In Figure 8 we show the HR diagram using the extinction- and distance-corrected Gaia DR2 BP<sub>0</sub>–RP<sub>0</sub> and G<sub>abs</sub> measurements. Here we show the measurements for HATS-71 as well as for all stars in the Gaia DR2 catalog in a  $10^{\circ} \times 10^{\circ}$  box centered on HATS-71 with parallax  $\varpi > 7$  mas,  $\sigma_{\varpi} < 0.2$  mas, and BP, RP,

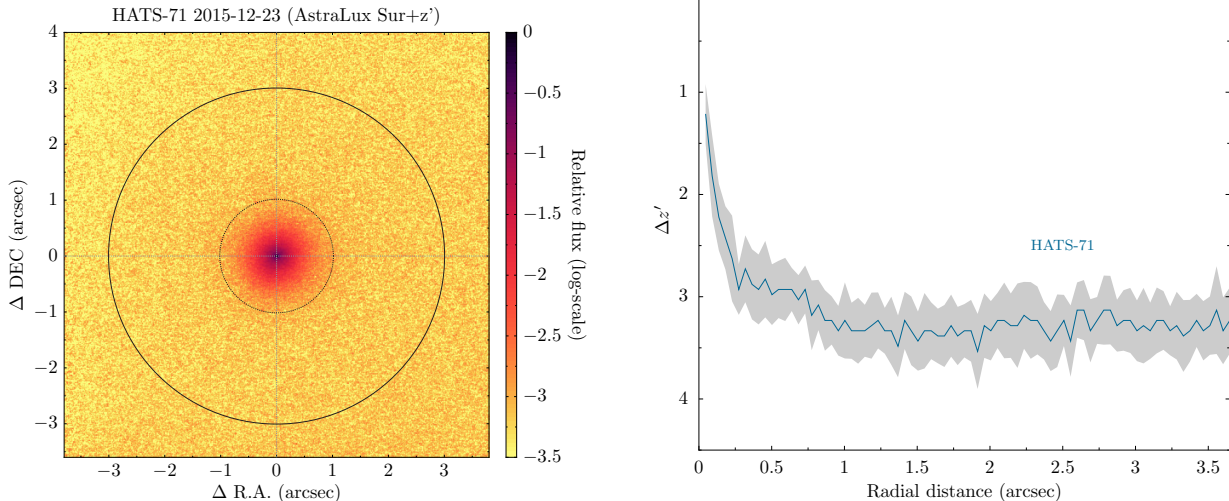


**Figure 7.** *Left:* Astralux Sur  $z'$  image of HATS-71 showing no apparent neighbors. *Right:*  $5\sigma$  contrast curve for HATS-71 based on our Astralux Sur  $z'$  observation. The gray band shows the variation in the limit in azimuth at a given radius.

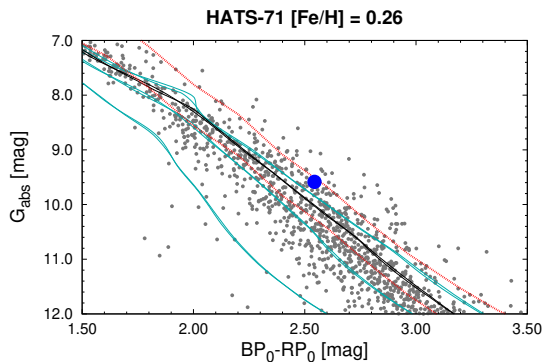


**Figure 8.** Hertzsprung-Russell diagram constructed from the Gaia DR2 photometry corrected for distance and extinction. The blue-filled circle shows HATS-71 (the uncertainties are smaller than the size of the circle), while the gray-filled circles show other stars in Gaia DR2 with  $\varpi < 7$  mas and within a  $10^\circ \times 10^\circ$  box centered on HATS-71. Overplotted are PARSEC model isochrones for metallicities of -0.5 (left set of cyan lines), 0 (middle set of cyan lines), +0.4414 (right set of cyan lines), and the spectroscopically estimated metallicity of 0.26 dex (black lines). At each metallicity we show models for ages 1.0 and 5.0 and 12.0 Gyr, though the difference with age at fixed metallicity is negligible at the scale shown here. We also show the median main sequence relation based on the Gaia DR2 stars included in the plot (left red line) and the sequence shifted upward in magnitude by 0.753 mag (right red line; this corresponds to equal-mass binary stars with both components falling on the median main sequence). HATS-71 lies near the upper red line, and above the +0.4414 dex isochrones, hinting that it may be an unresolved binary system.

and G all measured to greater than  $10\sigma$  confidence, and with  $1.5 < BP-RP_0 < 3.5$  and  $7.0 < G_{\text{abs}} < 12.0$ . We also show theoretical PARSEC isochrones for a range

of ages and metallicities, the median main sequence relation based on the selected stars from the Gaia DR2 sample, and the median main sequence shifted upward in magnitude by 0.753 mag (corresponding to equal-mass binary stars with both components falling on the median main sequence). As is apparent, HATS-71 falls above the highest metallicity theoretical relation calculated, and near the equal-mass binary sequence. This provides suggestive evidence that HATS-71 may be an unresolved binary star system, though we caution that there is no other spectroscopic or imaging evidence for such a companion. We consider how the inferred planetary and stellar parameters would change if there is an unresolved stellar companion in Section 3.2.

Previous work has shown that rapidly rotating, magnetically active M dwarfs often have cooler surface temperatures and larger radii than predicted by theoretical stellar evolution models (e.g., see the recent work by Jaehnig et al. 2018 and Somers & Stassun 2017 investigating the inflation of M dwarfs in the Hyades and Pleiades; see also references therein for a rich literature on this topic). HATS-71, however, does not exhibit  $H\alpha$  emission typical of magnetically active M dwarfs, and its measured photometric rotation period of  $41.72 \pm 0.14$  days (Section 2.1) is substantially longer than the periods of M dwarf stars for which radius inflation is typically observed ( $P_{\text{rot}} \lesssim 10$  days).

The measured astrometric, spectroscopic and photometric parameters of HATS-71 are collected in Table 2. Table 3 gives the stellar parameters that are derived through the modelling discussed in this Section, while Table 4 gives the planetary parameters derived through this modeling. The parameters listed under the “Single Star” columns in each table are those derived here under

the assumption that HATS-71 is a single star without a stellar binary companion.

We find that, thanks to Gaia DR2, the star HATS-71 has a tightly constrained radius of  $0.5161^{+0.0053}_{-0.0099} R_{\odot}$ . This, combined with the measured bulk stellar density (from the transits) of  $5.80 \pm 0.31 \text{ g cm}^{-3}$ , gives a stellar mass of  $0.569^{+0.042}_{-0.069} M_{\odot}$ . For comparison, using the Delfosse et al. (2000) mass- $M_K$  relation gives an estimated stellar mass of  $0.455 M_{\odot}$ , while using the Benedict et al. (2016) mass- $M_K$  relation gives an estimated stellar mass of  $0.50 M_{\odot}$ , consistent with the value coming from Gaia DR2 and the mean density estimate.

We find that the planet HATS-71b has a radius of  $1.080 \pm 0.016 R_J$ . Due to the faintness of the source we are unable to determine the mass of the planet with greater than  $2\sigma$  confidence. Our modeling yields a mass of  $0.45 \pm 0.24 M_J$ , with a 95% confidence upper limit of  $M_p < 0.81 M_J$ . The planet has an estimated equilibrium temperature (assuming full redistribution of heat and zero albedo) of  $567.9^{+12.6}_{-6.6} \text{ K}$ .

The  $89 \text{ ms}^{-1}$  scatter in the PFS RV residuals is significantly larger than the median per-point uncertainty of  $17 \text{ ms}^{-1}$ . Given the limited number of RVs obtained we cannot say whether this is due to the planet having a significant eccentricity, stellar activity, additional planets in the system, or our underestimating the uncertainties in these low S/N spectra. In modeling the data we incorporated a jitter term, which we added in quadrature to the formal uncertainties, and varied in the fit. We find a jitter of  $91 \pm 42 \text{ ms}^{-1}$  is needed to explain the excess scatter. If the orbit is eccentric, the jitter could be as low as  $37 \text{ ms}^{-1}$ .

### 3.2. Blend Analysis

In order to rule out the possibility that HATS-71 is a blended stellar eclipsing binary system, we carried out a blend analysis of the photometric data following Hartman et al. (2018). In this analysis we model the photometric and spectroscopic observations of HATS-71 under four different scenarios: a single star with a planet (referred to as the H-p model following the nomenclature from Hartman et al. 2009), a hierarchical triple star system where the two fainter stars form an eclipsing binary (referred to as the H,S-s model), a blend between a bright foreground star and a fainter background eclipsing binary star system (referred to as the H,S-SBGEb model), and a bright star with a transiting planet and a fainter unresolved stellar companion (referred to as the H-p,s model).

We find that the best-fitting model is the H-p,s model which yields  $\Delta\chi^2 = -345, -278$  and  $-657$  compared to the best-fit H-p model, H,S-SBGEb and H,S-s models,

respectively. The H,S-s model is strongly disfavored, however the H,S-SBGEb provides a better fit to the data modeled in this analysis than the H-p model. As noted in Section 3.1 the PARSEC models do not reproduce the combined high-precision measurements of color, density and absolute magnitude that are available for HATS-71 assuming a single star, so it is perhaps not surprising that the H,S-SBGEb model can provide a better fit than the H-p model. The best-fit H,S-SBGEb model consists of a  $0.42 M_{\odot}$  foreground star blended with a  $0.44 + 0.12 M_{\odot}$  eclipsing binary at a distance modulus that is  $0.65 \text{ mag}$  greater than the foreground star, and we find that the primary star in the background binary can be at most only  $1 \text{ mag}$  fainter in apparent brightness than the foreground star. Based on the Astralux Sur imaging (Section 2.5) the projected separation between the foreground star and the background binary would have to be  $\lesssim 0''.05$ . This H,S-SBGEb model still fails to fit the observations to within the uncertainties, yielding, for example, a predicted parallax of  $6.93 \text{ mas}$  for the foreground star which differs from the measured value of  $7.103 \pm 0.043 \text{ mas}$  by  $4\sigma$ . What is more, we find that all of the H,S-SBGEb blend models which fit the observations as well as or better than the H-p model (i.e., have  $\Delta\chi^2 < 25$  compared to the H-p model) predict a significantly larger RV variation measured from the composite spectrum than observed (with RMS ranging from  $660 \text{ m s}^{-1}$  to  $1.2 \text{ km s}^{-1}$ ). Based on these factors we consider both the H,S-s and H,S-SBGEb models excluded, and conclude that HATS-71 is a confirmed transiting planet system.

Because the H-p,s model provides a significantly better fit to the data than the H-p model, we also list in Table 3 and Table 4 the stellar parameters (for both the primary and secondary stars) and the planetary parameters for the H-p,s model derived from a DEMCMC analysis. Based on this modeling, we find that the planetary host star HATS-71A has a mass of  $0.4651 \pm 0.0062 M_{\odot}$ , and a radius of  $0.4618 \pm 0.0057 R_{\odot}$ , while the unresolved binary star HATS-71B has a mass of  $0.243 \pm 0.013 M_{\odot}$  and a radius of  $0.2714 \pm 0.0099 R_{\odot}$ . The planet has a radius of  $1.032 \pm 0.010 R_J$  and a poorly determined mass of  $0.45 \pm 0.26 M_J$  (95% confidence upper limit of  $< 0.949 M_J$ ). Here we do not incorporate the RV observations directly into the modeling in this case, but instead determine an approximate scaling factor of  $1.16 \pm 0.23$ , which we apply to the value of  $K$  as determined in Section 3.1 for the single star modeling to account for the effective dilution in the measured orbital variation of the primary star due to the non-varying spectral features contributed by the secondary star. This scaling factor is calculated by simulating

blended spectral cross-correlation functions in the same manner as done in ruling out the H,S-S<sub>BGEB</sub> model, and we conservatively assume a 20% uncertainty. We then re-calculate all parameters that depend on K after applying this scaling.

We also find that HATS-71B would have  $\Delta G = 2.05$  mag,  $\Delta z = 1.77$  mag compared to HATS-71A. Based on the Astralux Sur observations (Section 2.5) the two stars would have to be separated by less than  $0''.1$ , implying a projected physical separation of less than 14 AU. Note that we also checked whether there was enough proper motion for HATS-71 to have moved between archival images, but the proper motion was too small to reveal anything by blinking the UK Schmidt image (1997) and the DK 1.5m telescope image (2014). The slight over-luminosity of HATS-71 could also be caused by being a very young M-dwarf. However, a query with BANYAN Sigma (Gagné et al. 2018) yields no matches, so the star is unlikely to be the member of a young association.

#### 4. DISCUSSION

The discovery of HATS-71b demonstrates that, at least in some cases, Jupiter-sized planets are able to form and migrate around stars with masses as low as HATS-71 ( $0.569^{+0.042}_{-0.069} M_{\odot}$ ). It remains to be seen whether such planets occur with the same frequency as they do around solar-type stars (i.e.  $0.43 \pm 0.05\%$ ; Fressin et al. (2013)), or if giant planet formation is rarer around low mass stars as predicted by core accretion theory (e.g. Laughlin et al. 2004; Liu et al. 2016). Figure 10 shows giant planet masses as a function of host star mass, for systems with measured planetary masses. HATS-71b is the giant planet with the lowest host star mass that has been discovered to-date. The sparsity of systems with host masses  $< 0.5 M_{\odot}$  is apparent from Figure 10, although this may just be an reflection of the fact that most of the surveys contributing to the discoveries shown did not monitor sufficient numbers of low mass stars. Over the next two years of HATSouth and *TESS* discoveries, we should gain a better statistical understanding of these systems.

The deep transits that these systems present makes photometric detection relatively robust in both the HATSouth and *TESS* survey data. Indeed, the 4.7% transit for HATS-71b makes this the deepest transit observed by a hot Jupiter (as defined in the Introduction). In Fig. 9 we show the transit depths of these planets as a function of period, where the depths were calculated from the  $R_p$  planetary radius,  $R_{\star}$  stellar radius,  $b$  impact parameter,  $e$  eccentricity and  $\omega$  argument of periastron of the orbit (whenever available), also taking

into account the grazing nature of some orbits. The second and third deepest transits are Qatar-4b (3.4%; Alsubai et al. 2017), and HATS-6b, (3.3%; Hartman et al. 2015).

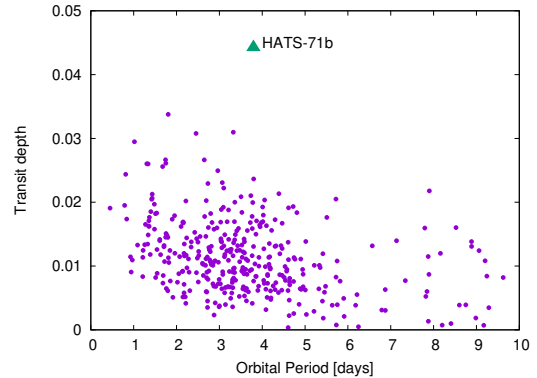


**Figure 9.** Transit depth as a function of orbital period for hot Jupiters. The depth was calculated from the  $R_p$  planetary radius,  $R_{\star}$  stellar radius,  $b$  impact parameter,  $e$  eccentricity and  $\omega$  argument of periastron of the orbit (whenever available), also taking into account the grazing nature of some orbits. Data was taken from [exoplanet.eu](http://exoplanet.eu).

However, radial velocity follow-up is extremely challenging since such stars are generally faint at visible wavelengths where most high precision spectrographs operate. The spectrum of these stars may also be less amendable to measuring precise radial velocity variations, as they are dominated by broader molecular absorption features rather than the narrow metal lines in solar-type stars (see Figure 3). A new generation of stable IR spectrographs will measure precise radial velocities in order to search for planets orbiting M-dwarfs, and these include CARMENES (Quirrenbach et al. 2014), SPIROU (Artigau et al. 2014), IRD (Kotani et al. 2014), HPF (Wright et al. 2018), NIRPS (Wildi et al. 2017) and GIARPS (Claudi et al. 2018).

This may provide another avenue for radial velocity follow-up of transiting giant planets orbiting M-dwarfs. However we note that for mid M-dwarfs such as HATS-71, optical spectroscopy will probably remain the best source of high precision radial velocities. For the CARMENES spectrograph, which hosts both an optical and IR arm, it appears that the radial velocity precision is still higher in the optical wavelengths until spectral types of M8 or later (Reiners et al. 2018).

The deep transits will facilitate atmospheric characterization of the planet using transmission spectroscopy. We estimate that the transmission signature could be anywhere from 300 ppm to 700 ppm, assuming the cloud properties of hot Jupiters around M stars are similar to those around F, G and K stars. Atmospheric character-

ization might be used instead of radial velocities to get the mass of the planet via MassSpec (de Wit & Seager 2013), although note the ambiguities detailed in Batalha et al. (2017).

HATS-71 was observed by the *TESS* spacecraft with 2 minute cadence as a candidate from the HATSouth Guest Observer Program (GO11214; PI Bakos). Due to the high precision ground-based light curves that had already been obtained in 2014 using 1 m-class telescopes (see Section 2.3), the addition of the *TESS* light curve did not have a significant impact on parameters such as the planetary radius or the orbital ephemerides. However the *TESS* light curve did contain the best photometry available at phase 0.5, which allowed us to rule out a secondary eclipse with much higher confidence. With many hundreds of transiting planet candidates, follow-up photometry that covers both the primary transit and any possible secondary eclipse is a time consuming and resource intensive task. The use of *TESS* light curves to help confirm existing candidates is therefore an obvious synergy between HATSouth and *TESS*, and this method will continue to be adopted for future *TESS* sectors.

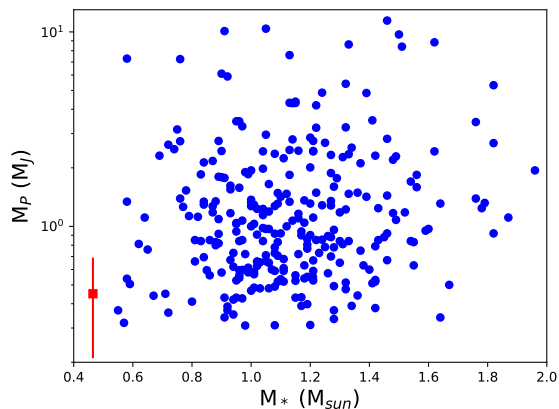


**Figure 10.** Planet mass as a function of host star mass for all known giant ( $M_p > 0.3 M_J$ ) planets with measured masses and radii (blue circles) and for HATS-71b (red square with errorbars). Data from NASA Exoplanet Archive as of 2018 October 4.

Development of the HATSouth project was funded by NSF MRI grant NSF/AST-0723074, operations have been supported by NASA grants NNX09AB29G, NNX12AH91H, and NNX17AB61G, and follow-up observations have received partial support from grant NSF/AST-1108686. G.Á.B wishes to thank Konkoly Observatory of the Hungarian Academy of Sciences for their warm hospitality during numerous visits during the past years, in particular the Distinguished Guest Fellow program. A.J. acknowledges support from FONDE-

CYT project 1171208, BASAL CATA AFB-170002, and project IC120009 “Millennium Institute of Astrophysics (MAS)” of the Millennium Science Initiative, Chilean Ministry of Economy. N.E. is supported by CONICYT-PCHA/Doctorado Nacional. R.B. acknowledges support from FONDECYT Post-doctoral Fellowship Project No. 3180246. N.E. acknowledges support from project IC120009 “Millennium Institute of Astrophysics (MAS)” of the Millennium Science Initiative, Chilean Ministry of Economy. L.M. acknowledges support from the Italian Minister of Instruction, University and Research (MIUR) through FFABR 2017 fund. L.M. acknowledges support from the University of Rome Tor Vergata through “Mission: Sustainability 2016” fund. V.S. acknowledges support from BASAL CATA PFB-06. A.V. is supported by the NSF Graduate Research Fellowship, Grant No. DGE 1144152.

Based on observations at Cerro Tololo Inter-American Observatory, National Optical Astronomy Observatory (NOAO Prop. ID 2016A/CN-615, 2016B-CN0908, 2017A-C79, 2017B-0909, 2018A-CN46/908; PI: Rabus), which is operated by the Association of Universities for Research in Astronomy (AURA) under a cooperative agreement with the National Science Foundation. M.R. acknowledges support from CONICYT project Basal AFB-170002.

This paper also makes use of observations from the LCOGT network. Some of this time was awarded by NOAO. We acknowledge the use of the AAVSO Photometric All-Sky Survey (APASS), funded by the Robert Martin Ayers Sciences Fund, and the SIMBAD database, operated at CDS, Strasbourg, France. This work has made use of data from the European Space Agency (ESA) mission *Gaia* (<https://www.cosmos.esa.int/gaia>), processed by the *Gaia* Data Processing and Analysis Consortium (DPAC, <https://www.cosmos.esa.int/web/gaia/dpac/consortium>). Funding for the DPAC has been provided by national institutions, in particular the institutions participating in the *Gaia* Multilateral Agreement. This research has made use of the NASA Exoplanet Archive, which is operated by the California Institute of Technology, under contract with the National Aeronautics and Space Administration under the Exoplanet Exploration Program. We acknowledge the use of TESS Alert data, which is currently in a beta test phase, from pipelines at the TESS Science Office and at the TESS Science Processing Operations Center. This paper includes data collected by the TESS mission, which are publicly available from the Mikulski Archive for Space Telescopes (MAST). Finally, G.Á.B. wishes to thank Princeton’s AST205 class for

all the inspiration they gave during the fall semester of 2018.

*Facilities:* HATSouth, ATT (WiFeS), Magellan:Clay (PFS), Blanco (ARCoIRIS), Danish 1.54m Telescope (DFOSC), LCOGT, NTT (Astralux Sur), TESS, Gaia, Exoplanet Archive

*Software:* FITSH (Pál 2012), BLS (Kovács et al. 2002), VARTOOLS (Hartman & Bakos 2016), CERES

(Brahm et al. 2017a), AstroImageJ (Collins & Kielkopf 2013; Collins et al. 2017), SPEX-tool (Cushing et al. 2004; Vacca et al. 2004), SExtractor (Bertin & Arnouts 1996), Astrometry.net (Lang et al. 2010), MWDUST (Bovy et al. 2016)

## REFERENCES

- Abbott, T. M. C., Walker, A. R., Points, S. D., et al. 2016a, in Proc. SPIE, Vol. 9906, Ground-based and Airborne Telescopes VI, 99064D
- Abbott, T. M. C., Walker, A. R., Points, S. D., et al. 2016b, in Proc. SPIE, Vol. 9906, Ground-based and Airborne Telescopes VI, 99064D
- Allard, F., Homeier, D., & Freytag, B. 2011, in Astronomical Society of the Pacific Conference Series, Vol. 448, 16th Cambridge Workshop on Cool Stars, Stellar Systems, and the Sun, ed. C. Johns-Krull, M. K. Browning, & A. A. West, 91
- Alsubai, K., Mislis, D., Tsvetanov, Z. I., et al. 2017, AJ, 153, 200
- Andersen, J., Andersen, M. I., Klougart, J., et al. 1995, The Messenger, 79, 12
- Artigau, É., Kouach, D., Donati, J.-F., et al. 2014, in Proc. SPIE, Vol. 9147, Ground-based and Airborne Instrumentation for Astronomy V, 914715
- Bakos, G. Á., Torres, G., Pál, A., et al. 2010, ApJ, 710, 1724
- Bakos, G. Á., Csubry, Z., Penev, K., et al. 2013, PASP, 125, 154
- Batalha, N. E., Kempton, E. M.-R., & Mbarek, R. 2017, ApJL, 836, L5
- Bayliss, D., Zhou, G., Penev, K., et al. 2013, AJ, 146, 113
- Bayliss, D., Gillen, E., Eigmüller, P., et al. 2018, MNRAS, 475, 4467
- Benedict, G. F., Henry, T. J., Franz, O. G., et al. 2016, AJ, 152, 141
- Bertin, E., & Arnouts, S. 1996, A&AS, 117, 393
- Bovy, J., Rix, H.-W., Green, G. M., Schlafly, E. F., & Finkbeiner, D. P. 2016, ApJ, 818, 130
- Brahm, R., Jordán, A., & Espinoza, N. 2017a, Publications of the Astronomical Society of the Pacific, 129, 034002
- Brahm, R., Jordán, A., Hartman, J., & Bakos, G. 2017b, MNRAS, 467, 971
- Brown, T. M., Baliber, N., Bianco, F. B., et al. 2013, PASP, 125, 1031
- Butler, R. P., Marcy, G. W., Williams, E., et al. 1996, PASP, 108, 500
- Claret, A. 2004, A&A, 428, 1001
- Claudi, R., Benatti, S., Carleo, I., et al. 2018, in Society of Photo-Optical Instrumentation Engineers (SPIE) Conference Series, Vol. 10702, 107020Z
- Collins, K., & Kielkopf, J. 2013, AstroImageJ: ImageJ for Astronomy, Astrophysics Source Code Library, , ascl:1309.001
- Collins, K. A., Kielkopf, J. F., Stassun, K. G., & Hessman, F. V. 2017, AJ, 153, 77
- Crane, J. D., Shtetman, S. A., & Butler, R. P. 2006, in Society of Photo-Optical Instrumentation Engineers (SPIE) Conference Series, Vol. 6269, 626931
- Crane, J. D., Shtetman, S. A., Butler, R. P., et al. 2010, in Society of Photo-Optical Instrumentation Engineers (SPIE) Conference Series, Vol. 7735, Society of Photo-Optical Instrumentation Engineers (SPIE) Conference Series
- Crane, J. D., Shtetman, S. A., Butler, R. P., Thompson, I. B., & Burley, G. S. 2008, in Ground-based and Airborne Instrumentation for Astronomy II, Vol. 7014, 701479
- Cushing, M. C., Vacca, W. D., & Rayner, J. T. 2004, PASP, 116, 362
- de Wit, J., & Seager, S. 2013, Science, 342, 1473
- Delfosse, X., Forveille, T., Ségransan, D., et al. 2000, A&A, 364, 217
- Dopita, M., Hart, J., McGregor, P., et al. 2007, Ap&SS, 310, 255
- Espinoza, N., Bayliss, D., Hartman, J. D., et al. 2016, AJ, 152, 108
- Fressin, F., Torres, G., Charbonneau, D., et al. 2013, ApJ, 766, 81
- Gagné, J., Mamajek, E. E., Malo, L., et al. 2018, ApJ, 856, 23
- Gaia Collaboration, Prusti, T., de Bruijne, J. H. J., et al. 2016, A&A, 595, A1

- Gaia Collaboration, Brown, A. G. A., Vallenari, A., et al. 2018, *A&A*, 616, A1
- Hansen, B. M. S., & Barman, T. 2007, *ApJ*, 671, 861
- Hartman, J. D., & Bakos, G. Á. 2016, *Astronomy and Computing*, 17, 1
- Hartman, J. D., Bakos, G. Á., Torres, G., et al. 2009, *ApJ*, 706, 785
- Hartman, J. D., Bayliss, D., Brahm, R., et al. 2015, *AJ*, 149, 166
- Hartman, J. D., Bakos, G. A., Bayliss, D., et al. 2018, *ArXiv e-prints*, arXiv:1809.01048
- Hippler, S., Bergfors, C., Brandner Wolfgang, et al. 2009, *The Messenger*, 137, 14
- Huang, C. X., Burt, J., Vanderburg, A., et al. 2018, *ArXiv e-prints*, arXiv:1809.05967
- Jaehnig, K., Somers, G., & Stassun, K. 2018, *ArXiv e-prints*, arXiv:1811.06561
- Jenkins, J. M., Twicken, J. D., McCauliff, S., et al. 2016, in *Society of Photo-Optical Instrumentation Engineers (SPIE) Conference Series*, Vol. 9913, *Software and Cyberinfrastructure for Astronomy IV*, 99133E
- Johnson, J. A., Aller, K. M., Howard, A. W., & Crepp, J. R. 2010, *PASP*, 122, 905
- Johnson, J. A., Gazak, J. Z., Apps, K., et al. 2012, *AJ*, 143, 111
- Jordán, A., Brahm, R., Bakos, G. Á., et al. 2014, *AJ*, 148, 29
- Kaufer, A., & Pasquini, L. 1998, in *Society of Photo-Optical Instrumentation Engineers (SPIE) Conference Series*, Vol. 3355, *Optical Astronomical Instrumentation*, ed. S. D'Odorico, 844–854
- Kotani, T., Tamura, M., Suto, H., et al. 2014, in *Proc. SPIE*, Vol. 9147, *Ground-based and Airborne Instrumentation for Astronomy V*, 914714
- Kovács, G., Bakos, G., & Noyes, R. W. 2005, *MNRAS*, 356, 557
- Kovács, G., Zucker, S., & Mazeh, T. 2002, *A&A*, 391, 369
- Lang, D., Hogg, D. W., Mierle, K., Blanton, M., & Roweis, S. 2010, *AJ*, 139, 1782
- Latham, D. W., Mazeh, T., Stefanik, R. P., Mayor, M., & Burki, G. 1989, *Nature*, 339, 38
- Laughlin, G., Bodenheimer, P., & Adams, F. C. 2004, *ApJL*, 612, L73
- Liu, B., Zhang, X., & Lin, D. N. C. 2016, *ApJ*, 823, 162
- Madhusudhan, N. 2018, *ArXiv e-prints*, arXiv:1808.04824
- Mandel, K., & Agol, E. 2002, *ApJL*, 580, L171
- Marigo, P., Girardi, L., Bressan, A., et al. 2017, *ApJ*, 835, 77
- Mordasini, C., Alibert, Y., Benz, W., Klahr, H., & Henning, T. 2012, *A&A*, 541, A97
- Newton, E. R., Charbonneau, D., Irwin, J., & Mann, A. W. 2015, *ApJ*, 800, 85
- Obermeier, C., Koppenhoefer, J., Saglia, R. P., et al. 2016, *A&A*, 587, A49
- Pál, A. 2012, *MNRAS*, 421, 1825
- Penev, K., Bakos, G. Á., Bayliss, D., et al. 2013, *AJ*, 145, 5
- Quirrenbach, A., Amado, P. J., Caballero, J. A., et al. 2014, in *Proc. SPIE*, Vol. 9147, *Ground-based and Airborne Instrumentation for Astronomy V*, 91471F
- Rabus, M., Jordán, A., Hartman, J. D., et al. 2016, *AJ*, 152, 88
- Reiners, A., Zechmeister, M., Caballero, J. A., et al. 2018, *A&A*, 612, A49
- Ricker, G. R., Winn, J. N., Vanderspek, R., et al. 2015, *Journal of Astronomical Telescopes, Instruments, and Systems*, 1, 014003
- Smith, J. C., Stumpe, M. C., Van Cleve, J. E., et al. 2012, *PASP*, 124, 1000
- Somers, G., & Stassun, K. G. 2017, *AJ*, 153, 101
- Southworth, J. 2011, *MNRAS*, 417, 2166
- Stassun, K. G., Corsaro, E., Pepper, J. A., & Gaudi, B. S. 2018, *AJ*, 155, 22
- Stumpe, M. C., Smith, J. C., Catanzarite, J. H., et al. 2014, *PASP*, 126, 100
- Vacca, W. D., Cushing, M. C., & Rayner, J. T. 2004, *PASP*, 116, 352
- Wheatley, P. J., West, R. G., Goad, M. R., et al. 2018, *MNRAS*, 475, 4476
- Wildi, F., Blind, N., Reshetov, V., et al. 2017, in *Society of Photo-Optical Instrumentation Engineers (SPIE) Conference Series*, Vol. 10400, *Society of Photo-Optical Instrumentation Engineers (SPIE) Conference Series*, 1040018
- Wright, J. T., Mahadevan, S., Hearty, F., et al. 2018, in *American Astronomical Society Meeting Abstracts*, Vol. 231, *American Astronomical Society Meeting Abstracts #231*, 246.45
- Zacharias, N., Finch, C. T., Girard, T. M., et al. 2013, *AJ*, 145, 44
- Zechmeister, M., & Kürster, M. 2009, *A&A*, 496, 577
- Ziegler, C., Law, N. M., Baranec, C., et al. 2018, *ArXiv e-prints*, arXiv:1806.10142
- Zucker, S., Mazeh, T., Santos, N. C., Udry, S., & Mayor, M. 2003, *A&A*, 404, 775



**Table 2.** Astrometric, Spectroscopic and Photometric parameters for HATS-71

Parameter	Value	Source
Astrometric properties and cross-identifications		
2MASS-ID .....	01021226-6145216	
TIC-ID .....	TIC 234523599	
Gaia DR2-ID .....	4710594412266148352	
R.A. (J2000) .....	01 <sup>h</sup> 02 <sup>m</sup> 12.2812s	Gaia DR2
Dec. (J2000) .....	−61°45′21.6599″	Gaia DR2
$\mu_{\text{R.A.}}$ (mas yr <sup>−1</sup> ) .....	78.858 ± 0.087	Gaia DR2
$\mu_{\text{Dec.}}$ (mas yr <sup>−1</sup> ) .....	−27.095 ± 0.064	Gaia DR2
parallax (mas) .....	7.103 ± 0.043	Gaia DR2
Spectroscopic properties		
$T_{\text{eff}\star}$ (K) .....	3500 ± 120	ARCoIRIS <sup>a</sup>
[Fe/H] .....	0.26 ± 0.13	ARCoIRIS
$\gamma_{\text{RV}}$ (m s <sup>−1</sup> ) .....	24.1 ± 1.4	WiFeS <sup>b</sup>
Photometric properties		
$P_{\text{rot}}$ (days) .....	41.72 ± 0.14	HATSouth
$G$ (mag) <sup>c</sup> .....	15.35120 ± 0.00050	Gaia DR2
$BP$ (mag) <sup>c</sup> .....	16.7435 ± 0.0038	Gaia DR2
$RP$ (mag) <sup>c</sup> .....	14.1873 ± 0.0013	Gaia DR2
$g$ (mag) .....	17.105 ± 0.042	APASS <sup>d</sup>
$r$ (mag) .....	15.8100 ± 0.0090	APASS <sup>d</sup>
$i$ (mag) .....	14.575 ± 0.031	APASS <sup>d</sup>
$J$ (mag) .....	12.605 ± 0.026	2MASS
$H$ (mag) .....	11.972 ± 0.032	2MASS
$K_s$ (mag) .....	11.727 ± 0.025	2MASS

<sup>a</sup> “Astronomy Research using the Cornell Infra Red Imaging Spectrograph” (ARCoIRIS) instrument on the Blanco 4 m at CTIO (Abbott et al. 2016b).

<sup>b</sup> The error on  $\gamma_{\text{RV}}$  is determined from the orbital fit to the RV measurements, and does not include the systematic uncertainty in transforming the velocities to the IAU standard system. The velocities have not been corrected for gravitational redshifts.

<sup>c</sup> The listed uncertainties for the Gaia DR2 photometry are taken from the catalog. For the analysis we assume additional systematic uncertainties of 0.002 mag, 0.005 mag and 0.003 mag for the G, BP and RP bands, respectively.

<sup>d</sup> From APASS DR6 for as listed in the UCAC 4 catalog (Zacharias et al. 2013).

**Table 3.** Derived stellar parameters for HATS-71 system

Parameter	Value	Value
	Single Star	Binary Star
Planet Hosting Star HATS-71A		
$M_{\star}$ ( $M_{\odot}$ )	$0.569^{+0.042}_{-0.069}$	$0.4651 \pm 0.0062$
$R_{\star}$ ( $R_{\odot}$ )	$0.5161^{+0.0053}_{-0.0099}$	$0.4618 \pm 0.0057$
$\log g_{\star}$ (cgs)	$4.766 \pm 0.027$	$4.7763 \pm 0.0063$
$\rho_{\star}$ ( $\text{g cm}^{-3}$ )	$5.80 \pm 0.31$	$6.65 \pm 0.17$
$L_{\star}$ ( $L_{\odot}$ )	$0.02702 \pm 0.00035$	$0.02249 \pm 0.00053$
$T_{\text{eff}\star}$ (K)	$3254 \pm 22$	$3294.3 \pm 4.3$
[Fe/H] (dex)	$0.237 \pm 0.063$	$0.305 \pm 0.036$
Age (Gyr)	...	$7.7^{+3.5}_{-4.8}$
$A_V$ (mag)	$0.032 \pm 0.011$	$0.032 \pm 0.011$
Distance (pc)	$140.68 \pm 0.83$	$140.75 \pm 0.86$
Binary Star Companion HATS-71B		
$M_{\star}$ ( $M_{\odot}$ )	...	$0.243 \pm 0.013$
$R_{\star}$ ( $R_{\odot}$ )	...	$0.2714 \pm 0.0099$
$\log g_{\star}$ (cgs)	...	$4.9575 \pm 0.0097$
$L_{\star}$ ( $L_{\odot}$ )	...	$0.00473 \pm 0.00058$
$T_{\text{eff}\star}$ (K)	...	$2912 \pm 37$

NOTE— The listed parameters for the “Single Star” model are those determined through the joint differential evolution Markov Chain analysis described in Section 3.1, while the “Binary Star” model parameters are determined as described in Section 3.2. Systematic errors in the bolometric correction tables or stellar evolution models are not included, and likely dominate the error budget. The “Single Star” values are determined based on an empirical method, while the “Binary Star” values make use of stellar evolution models. In the latter case, the constraint from these models leads to very low formal uncertainties on parameters such as  $T_{\text{eff}\star}$ .

Table 4. Orbital and planetary parameters for HATS-71b

Parameter	Value	Value
	Single Star	Binary Star
Light curve parameters		
$P$ (days)	$3.7955213 \pm 0.0000011$	$3.7955203 \pm 0.0000012$
$T_C$ (BJD) <sup>a</sup>	$2457699.38939 \pm 0.00020$	$2457699.38955 \pm 0.00024$
$T_{14}$ (days) <sup>a</sup>	$0.08622 \pm 0.00077$	$0.08612 \pm 0.00044$
$T_{12} = T_{34}$ (days) <sup>a</sup>	$0.01686 \pm 0.00067$	$0.01629 \pm 0.00020$
$a/R_\star$	$16.41 \pm 0.29$	$17.17 \pm 0.15$
$\zeta/R_\star$ <sup>b</sup>	$28.74 \pm 0.18$	$28.63 \pm 0.17$
$R_p/R_\star$	$0.2155 \pm 0.0017$	$0.2297 \pm 0.0031$
$b^2$	$0.108^{+0.035}_{-0.034}$	$0.013^{+0.015}_{-0.011}$
$b \equiv a \cos i/R_\star$	$0.329^{+0.050}_{-0.056}$	$0.112^{+0.053}_{-0.068}$
$i$ (deg)	$88.85 \pm 0.18$	$89.63 \pm 0.18$
Limb-darkening coefficients <sup>c</sup>		
$c_{1,r}$	0.5401	0.4738
$c_{2,r}$	0.2354	0.2970
$c_{1,R}$	0.4889	0.4237
$c_{2,R}$	0.2566	0.3158
$c_{1,i}$	0.3460	0.2798
$c_{2,i}$	0.3337	0.3962
$c_{1,I}$	0.3128	0.2513
$c_{2,I}$	0.3638	0.4265
RV parameters <sup>d</sup>		
$K$ (m s <sup>-1</sup> )	$87 \pm 44$	$98 \pm 56$
RV jitter PFS (m s <sup>-1</sup> ) <sup>e</sup>	$91 \pm 42$	...
Planetary parameters		
$M_p$ ( $M_J$ )	$0.45 \pm 0.24$	$0.45 \pm 0.26$
$R_p$ ( $R_J$ )	$1.080 \pm 0.016$	$1.032 \pm 0.010$
$C(M_p, R_p)$ <sup>f</sup>	0.05	...
$\rho_p$ (g cm <sup>-3</sup> )	$0.44 \pm 0.23$	$0.51 \pm 0.29$
$\log g_p$ (cgs)	$2.98^{+0.19}_{-0.27}$	$3.02^{+0.21}_{-0.29}$
$a$ (AU)	$0.03946^{+0.00095}_{-0.00168}$	$0.03689 \pm 0.00016$
$T_{\text{eq}}$ (K)	$567.9^{+12.6}_{-6.6}$	$562.0 \pm 2.3$
$\Theta$ <sup>g</sup>	$0.059 \pm 0.030$	$0.069 \pm 0.039$
$\log_{10}(F)$ (cgs) <sup>h</sup>	$7.373^{+0.038}_{-0.020}$	$7.3520 \pm 0.0071$

NOTE— Parameters in the “Single Star” column are determined as described in Section 3.1 assuming HATS-71 is a single star with a transiting planet. Parameters listed in the “Binary Star” column are determined as described in Section 3.2 assuming HATS-71 is an unresolved binary star with a transiting planet around one component. In both cases we assume the orbit is circular.

<sup>a</sup> Times are in Barycentric Julian Date computed on the TDB system with correction for leap seconds.  $T_C$ : Reference epoch of mid transit that minimizes the correlation with the orbital period.  $T_{12}$ : total transit duration, time between first to last contact;  $T_{12} = T_{34}$ : ingress/egress time, time between first and second, or third and fourth contact.

<sup>b</sup> Reciprocal of the half duration of the transit used as a jump parameter in our MCMC analysis in place of  $a/R_\star$ . It is related to  $a/R_\star$  by the expression  $\zeta/R_\star = a/R_\star(2\pi(1 + e \sin \omega))/(P\sqrt{1 - b^2}\sqrt{1 - e^2})$  (Bakos et al. 2010).

<sup>c</sup> Values for a quadratic law, adopted from the tabulations by Claret (2004). For the “Single Star” model these are fixed according to the spectroscopic parameters determined from the ARCoIRIS spectrum. For the “Binary Star” model these are varied at each step in the Markov Chain as the atmospheric parameters of the model star are varied, here we list the median parameter values. For the *TESS* light curves we assume the *I*-band limb darkening coefficients on the grounds that the unfiltered *TESS* bandpass is dominated by light from that portion of the spectrum for this M dwarf.

<sup>d</sup> The “Binary Star” model value for  $K$  is based on the “Single Star” model value scaled by a factor of  $1.16 \pm 0.23$  to account for dilution from the binary star companion as described in Section 3.2.

<sup>e</sup> Term added in quadrature to the formal RV uncertainties for each instrument. This is treated as a free parameter in the fitting routine for the “Single Star” model.

<sup>f</sup> Correlation coefficient between the planetary mass  $M_p$  and radius  $R_p$  estimated from the posterior parameter distribution. This was not estimated for the “Binary Star” model.

<sup>g</sup> The Safronov number is given by  $\Theta = \frac{1}{2}(V_{\text{esc}}/V_{\text{orb}})^2 = (a/R_p)(M_p/M_\star)$  (see Hansen & Barman 2007).

<sup>h</sup> Incoming flux per unit surface area, averaged over the orbit.

**Table 5.** Relative radial velocities and bisector spans from PFS/Magellan for HATS-71.

BJD (2,450,000+)	RV <sup>a</sup> (m s <sup>-1</sup> )	$\sigma_{RV}$ <sup>b</sup> (m s <sup>-1</sup> )	BS (m s <sup>-1</sup> )	$\sigma_{BS}$ (m s <sup>-1</sup> )	Phase
7022.57729	41.90	16.56	-264.3	1123.8	0.681
7025.56597	-46.25	15.91	-816.3	1469.2	0.469
7026.58472	...	...	33.9	932.1	0.737
7325.69973	-105.95	19.13	...	...	0.545
7385.55818	-69.45	17.33	6.7	970.8	0.315
7614.83615	189.26	17.52	-220.5	358.3	0.723
7616.85346	19.70	15.83	2859.9	969.4	0.254
7766.54828	120.67	22.78	3214.5	2049.4	0.694

<sup>a</sup> The zero-point of these velocities is arbitrary. An overall offset  $\gamma$  fitted to the velocities has been subtracted.

<sup>b</sup> Internal errors excluding the component of astrophysical jitter considered in Section 3.1.